Macromolecules
ARTICLE

Macromolecules **2009**, *42*, 4651–4660 **4651**
DOI: 10.1021/ma900021w

Bimodal Temperature Behavior of Structure and Mobility in High Molecular Weight P3HT Thin Films

Siddharth Joshi,[†] Patrick Pingel,[‡] Souren Grigorian,*[†,] Tobias Panzner,[†] Ullrich Pietsch,[†] Dieter Neher,[‡] Michael Forster,[§] and Ullrich Scherf[§]

[†]*Solid State Physics, University of Siegen, Walter Flex Strasse 3, D-57068, Siegen, Germany,* [‡]*Institute of Physics and Astronomy, University of Potsdam, Karl-Liebknecht-Strasse 24-25, D-14476 Potsdam, Germany, and* [§]*Macromolecular Chemistry, University of Wuppertal, Gauss-Strasse 20, D-42097 Wuppertal, Germany*

Received January 6, 2009; Revised Manuscript Received May 15, 2009

ABSTRACT: We report a temperature dependent crystalline structure of spin-coated thin films of high molecular weight regioregular poly(3-hexylthiophene) (P3HT) ($M_n \sim 30000$ g/mol) and its correlation with charge carrier mobility. These investigations show a reversible change of the crystalline structure, where the interlayer lattice spacing (100) along the alkyl side chains continuously increases up to a temperature of about 220 °C; in contrast, the in-plane $\pi-\pi$ distance reduces with increasing temperature. These changes in structure are reversible and can be repeated several times. The temperature-induced structural properties differ for thick and thin films, pointing to a surface/interface role in stabilization of the layer morphology. In contrast to the structural changes, the carrier mobility is rather constant in the temperature range from room temperature up to 100−120 °C, followed by a continuous decrease. For thick layers this drop is significant and the transistor performance almost vanishes at high temperature, however, it completely recovers upon cooling back to room temperature. The drop of the charge carrier mobility at higher temperatures is in contrast with expectations from the structural studies, considering the increase of crystalline fraction of the polycrystalline layer. Our electrical measurements underscore that the reduction of the macroscopic mobility is mostly caused by a pronounced decrease of the intergrain transport. The thermally induced crystallization along (100) direction and the creation of numerous small crystallites at the film−substrate interface reduce the number of long polymer chains bridging crystalline domains, which ultimately limits the macroscopic charge transport.

Introduction

Among many conjugated polymers, poly(3-alkylthiophenes) (P3ATs), a class of organic semiconductors with good solubility and processability and environmental stability accompanied by a high charge-carrier mobility, have been found. This makes the material potentially useful for fabricating inexpensive, flexible, and large-area electronic devices. Potential applications include organic light emitting diodes, nonlinear optical devices, rechargeable batteries, and organic field-effect transistors (OFETs).[1,2] In particular, thiophene-based polymers have shown field-effect mobilities between 0.1 and 0.5 $cm^2 V^{-1} s^{-1}$,[3−5] which approaches a-Si mobility of 1.0 $cm^2 V^{-1} s^{-1}$.

Typically, solution-processed polymers form complex microstructures that are deposited to form a thin film on top of a solid substrate. In the case of poly(3-hexylthiophene), P3HT, it was found that the polymer chains self-organize into a well-ordered structure for a broad range of molecular weights ($M_w = 2500-30000$ g/mol).[6−11] Depending on the preparation conditions and molecular parameters, these *nanofibrils* can spatially extend up to several micrometers in lengths and few hundred nanometers in width. Under different conditions, P3HT molecules can arrange into crystalline domains with an isotropic size of 10−100 nm.[6,12−15] However, in both cases the fibrillar structures or the crystalline nanodomains are separated by a significant and often underestimated amount of amorphous material which is presumably formed by expelled segments during chain folding and chain ends.[7,15−18] Note that thin film crystallization depends subtly on processing conditions and molecular parameters such as molecular weight, regioregularity, and polydispersity. For a P3HT fraction with very low molecular weight and moderate polydispersity we previously found the formation of mostly amorphous films, in which sharply distinguished crystallites are embedded.[7,8,16] On the other hand, it has been found that low molecular weight films of a polythiophene derivative (PQT-12) with a very low polydispersity are highly crystalline with a lateral coherence in the range of a micrometer and a high field-effect mobility.[19]

It is generally accepted, that charge carrier mobility in polymer thin films is a function of molecular weight.[8,12] At the same time, Meijer et al.,[13] have shown that there can be a molecular weight optimum for the order parameters in fluorene-type copolymers and the picture of a simple increase in order with increasing molecular weight may be not true for all cases. For P3HT, the charge carrier mobility was found to increase by 4 orders of magnitude changing molecular weight between 3000 and 30000 g/mol. This was particularly interpreted in terms of better connectivity of high-mobility crystalline domains by long polymer chains in high molecular weight samples. Extending the model to the previously mentioned low molecular weight polythiophenes, we found that the degree of crystallinity—defined as the volume portion of polymer chains and segments which are arranged in an ordered fashion − is a major parameter for charge carrier mobility and that the amorphous phase ultimately limits the charge transport in thin polymer films.

*To whom correspondence should be addressed. E-mail: grigorian@physik.uni-siegen.de.

Published on Web 06/11/2009

Charge transport in OFETs was shown to depend strongly on the orientation of the crystalline domains.[3,13] The optimal orientation corresponds to the plane of the conjugated rings being parallel to the film−substrate interface.

The morphologies of thin films that were prepared from solution by spin-coating or other low-cost procedures are not in equilibrium. Subsequently, annealing is a necessary technological step in order to enhance the built-in performance of the polymer. The effect of annealing P3HT thin films in OFET devices was reported for the first time by Abdou et al.[20] They found significant improvement in the OFET characteristics after annealing P3HT thin films at 180 °C in N_2-atmosphere. Zen et al.[9] annealed the P3HT thin films at about 150 °C for 5 min and correspondingly found an increase of mobility by a factor of 2 compared to pristine samples. A similar gain was reported by Grecu et al., for pure SiO_2 and OTS-treated surfaces,[21] which was explained by the improved film morphology due to a reduction of trapped solvent within the volume. Bao et al. found that treating a film with ammonia or heating to 100 °C under N_2 can increase the on/off ratio without decreasing the mobility.[22] So far, few papers have dealt with a systematic investigation of the correlation between thin film morphology and electrical properties of alkyl-substituted polythiophene films as a function of temperature.

Werzer et al.,[23] performed temperature dependent X-ray diffraction and reflectivity measurements for rr-P3HT with a molecular weight (M_w = 45000 g/mol)$^{-1}$ at various temperatures. They observed an increase of the (100) lattice spacing associated with an increase of total film thickness of 15%. The full width half-maximum (fwhm) of the peak was decreased and the intensity increased up to 150 °C, followed by a decrease of intensity, and a complete disappearance at 200 °C. Kim et al.[24] reported on a complete reorientation of molecules from an edge-on into a flat-on orientation with respect to substrate after annealing of P3HT films with a molecular weight of M_n = 30000 g/mol, M_w/M_n = 1.8, at 240 °C on OTS-treated surfaces.

Very recently, DeLongchamp et al.[25] correlated thermally induced reorganization of crystal structure with temperature dependent mobility in thin films of a thiophene-based copolymer pBTTT with dodecyl side-chains. They found significant improvement of mobility, after heating through a thermotropic mesophase transition, which they associate with a melting of interdigitated alkyl side chains, accompanied by an improved $\pi-\pi$ stacking of thiophene rings.

We have recently shown[7] that, for LMW P3HT (M_n ~2500 g/mol), the temperature behavior of the crystal structure is a function of film thickness. Whereas films with thickness on the order of ~200 nm show a continuous increase in (100) spacing up to the melting point at about 70 °C, the *d* spacing of thin films (10 nm thickness) is maintained up to a temperature close to the melting temperature, which is explained by the film−substrate interaction.

In this paper, we report on the morphology and electrical properties in HMW P3HT films as a function of temperature and with a depth resolution from the polymer surface toward the substrate. As for LMW films, the (100) lattice spacing is found to increase with increasing temperature up to the typical melting temperature. At the same time the in-plane (020) reflection shows a decrease of lattice spacing. Surprisingly, this shortening in $\pi-\pi$ distance does not lead to an increase of mobility; at elevated temperature, the field-effect mobility even drops down. Interestingly, both properties, the change in mobility and the *d*-spacing, are completely reversible upon a cycle of heating and cooling. We will show that this behavior is due to the growth of crystallites at high temperature at the cost of the chains in their vicinity from interconnecting neighboring crystallites.

In this paper, our studies are focused on X-ray investigations of the structure ordering and the surface-interface dependent structural modifications and thermal behavior of HMW P3HT films (M_n = 30000 g/mol), in particular, the analysis of the structural properties parallel and perpendicular to the film−substrate interface. We studied the polymer film structure as a function of film thickness and for different substrate treatments of the SiO_2 insulator. Finally, the structural parameters are related to electrical properties of thin film OFETs.

Experimental Section

High molecular weight (HMW) regioregular poly(3-hexylthiophene), rr-P3HT, was synthesized and prepared by previously described methods,[26,27] which gives a polymer fraction with a polydispersity index of 1.32. The regioregularity of the HMW P3HT is >98%, calculated with NMR spectroscopy. The molecular weight explored of HMW P3HT is M_n = 30000 g/mol, M_w = 40000 g/mol, having the polydispersity (M_w/M_n) = 1.32. All the thin-film samples (HMW fractions) were prepared by the spin-coating from chloroform solution. Variation of the film thickness was achieved by varying the solution concentration, keeping the speed of spin-coater fixed at 4000 rpm for 30 s. Usually the prepared films are homogeneous and uniform in thickness (see Supporting Information, Figure S1).

All of the samples for both structural analysis and mobility measurements were prepared on n-doped Si, covered with 300 nm thick thermally grown SiO_2. For the preparation of plain P3HT layers for structural analysis, three different types of surface treatments were employed prior to the deposition of the polymer. The first substrate type was only wet-cleaned in an ultrasonic bath with solvents (acetone, isopropanol), in the following termed as untreated. The other two were silanized immediately after ultrasonic treatment. Two types of silane molecules, hexamethyldisilazane (HMDS) and octadecyltrichlorosilane (OTS),[13,24] respectively, were used. The HMDS was deposited by spin coating using 10% HMDS/90% chloroform solution at 2000 rpm for 30 s. The OTS treatment was also done by spin coating a 10% OTS/90% chloroform solution at 2000 rpm for 30 s. To vary the thickness of the polymer layer, the concentration of P3HT in chloroform solution was varied; 1 mg/mL (thin samples) and 40 mg/mL (thick samples).

The thickness of the thin samples was measured by X-ray reflectivity and was always on the order of 10 nm. The thickness of the thick samples were assumed to be more than 200 nm; on the basis of our previous measurements, no thickness oscillations were found beyond the film thickness of 200 nm.

The X-ray diffraction measurements were carried out using synchrotron radiation at BW2 at Hasylab/Desy, Hamburg, Germany, using a wavelength λ = 1.24 Å, at BL9 station of DELTA (λ = 0.8267 Å) and at ID10b of ESRF (λ = 0.8236 Å). At DELTA, we used a circular image plate made of 3450 pixels in diameter, each pixel being 100×150 μm in size spaced 43 cm from the sample and probed with a beam size of 0.5×1.5 mm^2. At ESRF, we used a CCD camera with 2048×2048 pixels, each 65 μm in size set 30 cm from the sample. Here the beam size was 0.1 × 0.3 mm^2. A 1024 × 1024 pixels detector was used at Hasylab, where each pixel was of 60 μm in size. In all measurements the in-plane scattering angle is 2θ and the incident angle and the exit angle within the incident plane are α_i and α_f, respectively. For comparison of the measurements taken at different sources all angular coordinates are transformed into *q*-space.[7]

To limit the penetration depth of the probing X-ray to the film thickness, out-of plane and in-plane diffraction scans are performed for fixed incidence angles α_i, ranging between $\alpha_{cf} < \alpha_i < \alpha_{cs}$, where α_{cf} and α_{cs} are the critical angle of total external reflection of film and substrate, respectively, which depend on the material density and X-ray wavelength. Out-of plane scans were performed by keeping the angle of incident

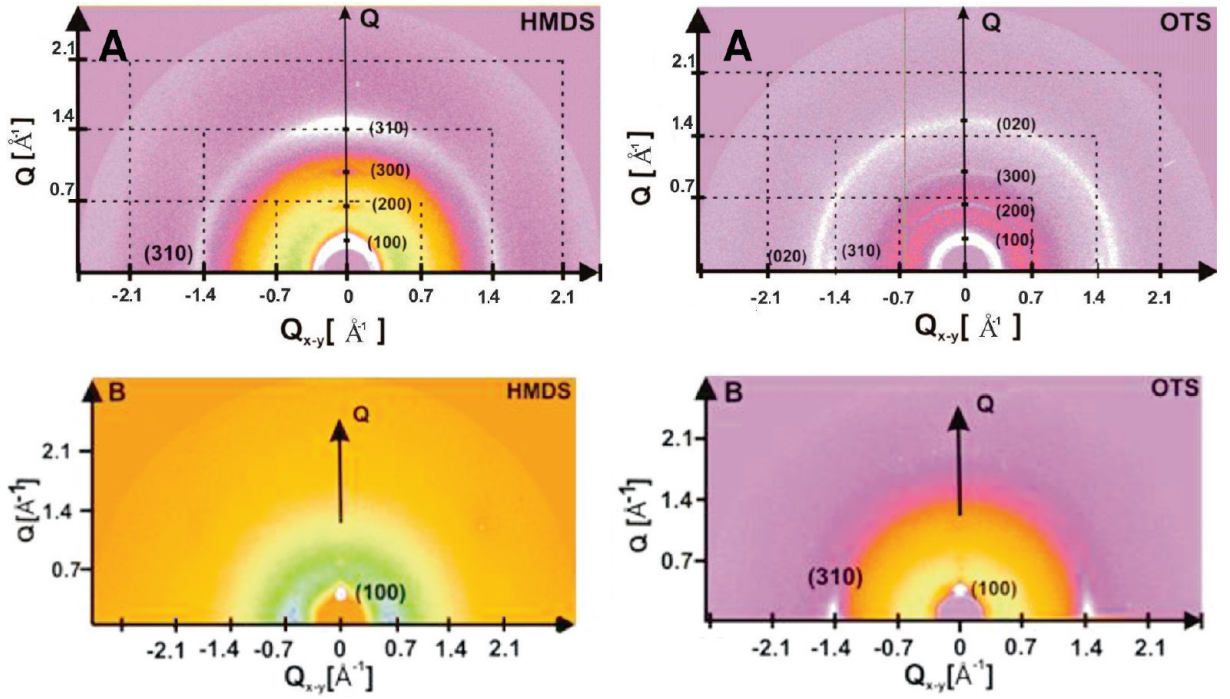

Figure 1. Image plate measurements of the original thick (A) and thin (B) P3HT layers with HMDS (left-hand side) and OTS (right-hand side) interface treatment at an angle of incidence $\alpha_i = 0.10°$.

Table 1. Film Thickness and Structural Parameters of P3HT Layers at Room Temperature

sample no.	sample	thickness t, (nm)	d_{100} (nm)	crystallite size L_c (nm)
1	40 mg/mL on HMDS	no thickness oscillation found	1.66 ± 0.02	9.0 ± 1.0
2	40 mg/mL on OTS	no thickness oscillation found	1.66 ± 0.02	9.7 ± 1.0
3	40 mg/mL on Si/SiO_2	no thickness oscillation found	1.63 ± 0.02	9.0 ± 1.0
4	1 mg/mL on HMDS	11 ± 0.5	1.73 ± 0.02	9.2 ± 1.1
5	1 mg/mL on OTS	12 ± 1	1.63 ± 0.02	9.05 ± 1.1
6	1 mg/mL on Si/SiO_2	11 ± 1	1.70 ± 0.02	8.2 ± 1.4

α_i constant, below the critical angle of substrate and alone α_f was scanned. The out-of-plane component of momentum transfer can be described by

$$Q = (2\pi/\lambda)(\sin\alpha_i + \sin\alpha_f) \approx (2\pi/\lambda)(\sin\alpha_f), \quad \text{for GOD} \tag{1}$$

Scanning of the in-plane 2θ angle at fixed α_i results in

$$Q_{x-y} \approx (2\pi/\lambda)\sqrt{1 + \cos^2\alpha_f - 2\cos\alpha_f \cos 2\theta} \approx (2\pi/\lambda)\left(\sin\frac{2\theta}{2}\right), \quad \text{for GID} \tag{2}$$

All X-ray measurements were performed under vacuum conditions ($\sim 10^{-3}$ mbar) using a DHS 900 domed hot stage provided by Anton Paar GmbH, Graz, Austria. This was crucial in order to avoid substantial radiation damage at the polymer sample and to reduce background and air scattering. For temperature-resolved measurements, the temperature was increased in steps from room temperature to the melting point ($T_m \sim 260$ °C) of the individual sample with an accuracy of ±0.5°. Data were taken after temperature stabilization at the surface of the sample. Temperature reduction was done using a slow but fixed cooling rate of about 4 °C/min followed by in-plane and out-of-plane measurements at room temperature again. In some cases a second and a third heating/cooling cycle was performed.

OFETs were prepared in the bottom-gate top-contacts geometry, on top of a n-doped Si substrate (see the supplement for more details).

Grazing Incidence X-ray Scattering

Overview. In the following subsections we report on the thin film morphology perpendicular and parallel to the substrate, using out-of-plane and in-plane geometry in X-ray grazing incidence diffraction (see, for example, ref 7). In-situ temperature-dependence of morphology and OFET properties will help us to understand the structural changes during and after annealing of P3HT thin films. Additionally, the effect of silanization of the SiO_2 surface on morphology and charge transport will be explored.

An overview of the studied samples on different insulators with the key parameters and thicknesses obtained from X-ray diffraction and reflectivity can be found in Table 1.

The typical scattering patterns from as-grown samples are shown in Figure 1 recorded by image plate exposure at room temperature at the Delta synchrotron source. Thick samples on both HMDS and OTS-coated substrates show a typical ring structure of wide angle reflections with a preferred orientation of (100) planes and interplanar distances determined by the hexyl chains. Here (h00) peaks appear with certain angular distribution increasing with h. In addition, the interchain $\pi-\pi$ stacking of about 3.8 Å can be associated with reflection from (0k0) planes. However, due to the lack of structural information, it is impossible to find unique solution for the unit cell.

The HMDS-treated thick film shows a textured feature in contrast to the OTS-coated sample. The higher intensity and broader fwhm of the so-called "mixed-indexing" peak (310) at roughly 1.4 $Å^{-1}$, could be due to the presence of the

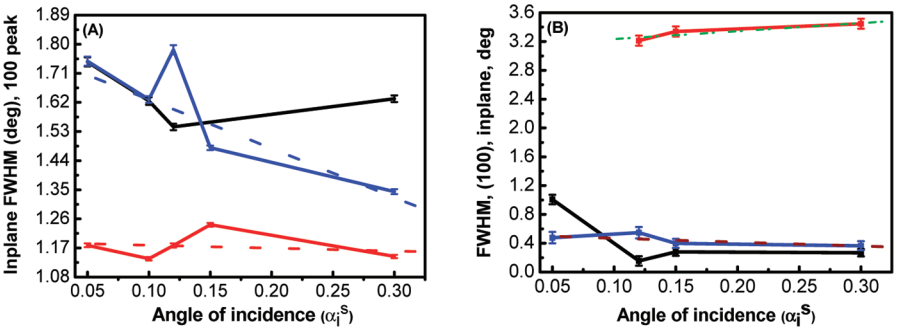

Figure 2. Depth dependence of the fwhm of the in-plane (100) peak at RT (black symbols), 200 °C (red symbols) and at RT after cooling (blue symbols) for thick (A) and thin (B) samples on an OTS-treated substrate.

number of peaks in very close vicinity. Therefore, combined intensity of the mixed peak can be higher with a broader fwhm; similar mixed reflections were found in ref 17.

For thick film on OTS-coated substrate there is a clear presence of (020) ring as well as in-plane peaks which are indexed as (310) reflections (Figure 1A, right). In contrast, for thick films on HMDS the (020) peak is not visible (Figure 1A, left). At the same time the (310) peak appears for both substrates either as a textured (HMDS) or as a sharp preferential peak along the in-plane direction (OTS). This could be the indication of tilting of the polymer chains in crystalline domains with preferential twisting of chains along the in-plane direction. In general, both samples indicate the presence of a mixed orientation (edge-on and flat-on) where edge-on is dominating across the whole thickness of film.

In contrast, thin film samples on both HMDS and OTS-coated substrates (Figure 1B) show a narrow angular distribution of the (*h*00) reflections. One can see the presence of spots rather than rings, which directly indicate the preferential orientation of nanocrystals along direction of the film normal (see later). Interestingly, (310) peaks are still present for OTS-treated films indicating strong influence of this insulator on the tilting of polymer chains. At the same time, as there is a clear absence of a (020) peak for both the HMDS and OTS cases, resulting in a rather weak ordering of $\pi-\pi$ stacking in thin films.

Different shapes of peaks (in particular, along Q) from 2D scattering images became visible due to the orientational distribution (OD) of the nanocrystallites. In the case of complete random orientations of crystallites the scattering pattern in Figure 1 shows closed Debye−Scherrer rings, preferential orientation would result in well pronounced single spots. Orientational freedom of nanodomains causes a rotation of the [100] diffraction vector with respect to the surface normal. Annealing can improve structural ordering and is usually used to improve the morphology from a random orientation to a well-ordered state. Such temperature-induced improvement of nanodomain orientation and influence on the size of crystalline nanodomains and intervening disordered regions was studied for a semiconducting pBTTT polymer.[28] Considering grazing-incidence the OD must be larger than the 2Θ angle of the respective reflection in order to see a spot along Q. However, the width of this peak seen along Q_{x-y} is a cut of this OD and visible changes seen in this cut are assumed to be proportional to possible changes of this OD. Keeping this relation in mind we used the projected width of the (100) reflection along Q_{x-y} to probe thermally induced changes in the OD close to the surface and toward the bulk tailoring with incidence angle from extremely shallow to a value larger than α_c. Neglecting instrumental resolution, the widths ΔQ_{x-y} of thick and thin films

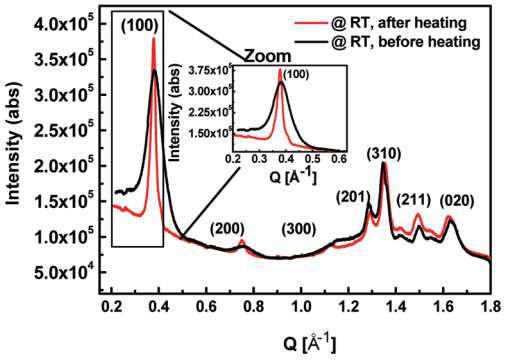

Figure 3. Out-of-plane scan of a thick P3HT layer on HMDS-treated SiO_2 for $\alpha_i = 0.15°$ before (black line) and after (red line) annealing.

shows different depth dependence in OD (Figure 2). Whereas the room temperature (RT) value of ΔQ_{x-y} is found to be same for all α_i, it varies for thick films. Here ΔQ_{x-y} is larger at surface but decreases toward the bulk; the bulk value ($\alpha_i = 0.3°$) is reduced after first temperature cycle. More remarkable is the difference for both films measured at 200 °C. Thin films show a much larger ΔQ_{x-y} compared to the RT value, which is found to be opposite for thick films. That means that OD becomes narrower for thick films but wider for thin films.

Thick Films. Out-of-Plane Measurements. The line scans along the normal direction ($Q = Q_{out}$) from a 2D scattering pattern (see Figure 1A) for a thick sample on HMDS-treated substrate before and after annealing are shown in Figure 3. In comparison to Figure 1 these data were collected using a point detector at ESRF providing much higher photon flux. It clearly shows that the (100) peak after the annealing step becomes narrower and higher in intensity compared to the as spun sample. Reflections at higher Q values are less affected. They show a very little peak shift with small changes in intensity and fwhm. This suggests that thermal treatment mostly affects the lamellar ordering along alkyl side chains and only has moderate influence on tilted polymer chains and $\pi-\pi$ stacking.

Indexing of Bragg peaks found in our measurements is based on a monoclinic unit cell similar to the one evaluated for LMW fraction.[7] In contrast to LMW fraction small modifications of unit cell for HMW fraction were considered by a slight increase of *a* and *b* lattice parameters corresponding to alkyl-chain spacing and $\pi-\pi$ stacking, respectively. Refinement of a structural model based only on few Bragg reflections results in several solutions matching all the measured peak positions in a similar manner. Out of these solutions a few mixed (*hkl*) matching one and the same Q-value were found. Therefore, we assumed the higher

intensity of (310) might originate from a coincidence of more than a single (*hkl*). Table 2 shows our proposed unit cells (D1 and D2). They have lattice parameters similar to ones found by other authors,[17,29,34] but with a slightly larger angle β between alkyl side chains and backbones.

As in the image plate measurements, we also noticed the presence of a (310) peak which is higher in intensity in comparison to the other high-Q peaks. Evidence of the preferential tilt of the polymer chains within crystalline lamellae and mixed reflections were recently observed by a high-resolution TEM technique in ref 17. On the basis of TEM observations, preferential tilt angles in nanocrystallites of the HMW fraction of regioregular P3HT were found, resulting in fold surfaces such as (110), (210), or (310).

Figure 4 shows the development of the (100) peak intensity during the first heating cycle for three different substrates (HMDS, OTS, SiO_2). Starting from RT, the intensity increases continuously up to a temperature of about 220 °C followed by sharp decrease of intensity due to crystal melting. The gain in intensity is between a factor of 2 and 10 for the investigated samples. Similar thermal behavior was found by Tashiro et al.,[29] where temperature-induced gain was in the relatively narrow 80−130 °C and broader 120−220 °C ranges for P3DT and P3HT films, respectively. This gain is accompanied by a shift in peak position toward a lower Q-value and decrease of the fwhm. Upon cooling back to RT, the (100) peak shifts back to the Q position of the original sample, ending up with a slightly higher intensity and reduced fwhm. However, after annealing the intensity at RT is much lower than at elevated temperatures in between 100 and 220 °C. Parts A and B of Figure 5 show the progress of the out-of-plane (100) peak during three subsequent heating and cooling cycles for two different incident angles α_i (0.05°, 0.30°) measured at samples similar to that shown in Figure 4. After the first cycle there is a significant gain in peak intensity. After the second and the third cycles, it is seen that the peak intensity switches back and forth between the two Q positions. Additionally, the peak intensities do not change anymore characterizing the appearance of thermal equilibrium state: saturation of crystalline domains growth and thermal expansion with increase of temperature. Such expansion is reproducible at both, low and high angles of incidence α_i (0.05°, 0.30°), i.e. in bulk as well as at the film surface, respectively. The increase of d-spacing and crystallite size perpendicular to the surface is shown in Figure 6 as a function of temperature. The crystallite size was calculated from the fwhm of the (100) Bragg peak using Scherrer's equation. The effects of crystal size and disorder can be unambiguously separated based on the Warren and Averbach approach. This technique was successfully applied for investigations of semicrystalline poly(3-dodecylthiophene) films considering up to fifth order (h00) reflections.[30] In the present case, in particular, for thin films, (h00) high order reflections were not accessible. Therefore, in our further study, we focus on thermally induced structural changes of first order reflection of alkyl side chain stacking. Using the changes of data on a relative scale, we found the d-value increases almost linearly until the melting temperature and the thermal expansion coefficient of $\alpha_T = \Delta d/(d\Delta T) = 4.7 \times 10^{-4}\ K^{-1}$ is almost independent of interface treatment (OTS, HMDS, or pure SiO_2). The crystal size grows from about

Table 2. Comparison of Inter-Planar Distances for Different Unit Cells[a]

hkl	*D*_obs (Å)	D1 (Å)	D2 (Å)	D3 (Å)	D4 (Å)	D5 (Å)
100	16.61	16.61	16.62	15.97	16.63	16.8
200	8.35	8.31	8.30	7.99	8.32	8.4
300	5.59	5.54	5.54	5.32	5.54	5.6
201	4.89	4.90	5.10	5.41		5.68
310	4.65	4.52	4.50	4.40	4.58	4.52
211	4.21	4.16	4.25	4.45	3.90	4.56
020	3.85	3.90	3.85	3.9	3.88	3.83

[a] On the basis of above cell structures, the following unit cell proposed: D1, present paper, monoclinic, a = 17.2, b = 7.8, c = 7.6, $\alpha = \gamma = 90°$, $\beta = 105°$; D2, present paper, monoclinic, a_1 = 16.9 b = 7.7, c = 7.6, $\alpha = \gamma = 90°$, $\beta = 100.7°$; D3, Brinkmann et al.,[16,17], monoclinic, a_1 = 16.0, a_2 = 7.8, a_3 = 7.8, $\gamma = 93 \pm 5°$, where all the d-spacing calculations were based on the proposed monoclinic unit cell; D4, Tashiro et al.,[29] orthorhombic, a = 16.63, b = 7.75, c = 7.77, where all the peaks d-spacing values were directly taken from the given table; D5, Prosa et al.,[34] orthorhombic, a = 16.8, b = 7.66, c = 7.70, where all the d-spacing calculations were based on proposed orthorhombic unit cell values; see additionally http://romano.physics.wisc.edu/winokur/handbook/node23.html#table2.

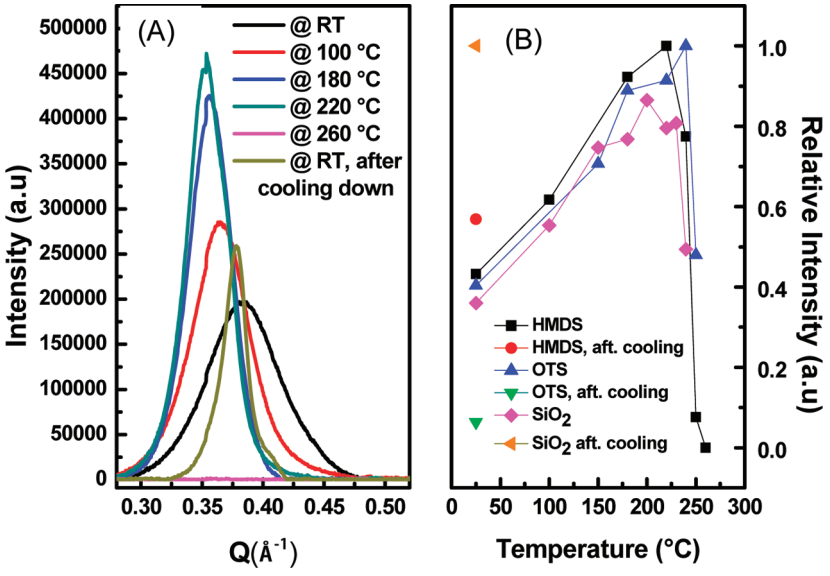

Figure 4. (A) Temperature dependent variation of the out-of-plane (100) peak for thick sample on HMDS-treated substrate for α_i = 0.15° and (B) change of peak intensity as a function of temperature for all three substrates HMDS (black), OTS (blue), and SiO_2 (magenta) followed by the obtained intensity after cooling back to RT, HMDS (red), OTS (green), and SiO_2 (orange).

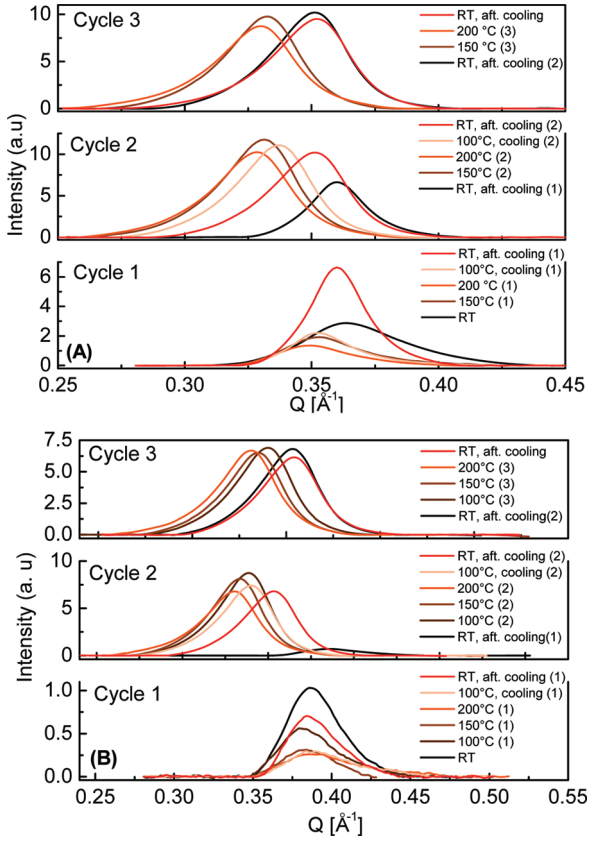

Figure 5. Temperature dependence of the out-of-plane (100) peak during three cycles of heating and cooling for a thick P3HT layer on a HMDS-treated substrate for $\alpha_i = 0.05°$ (A) and 0.30° (B).

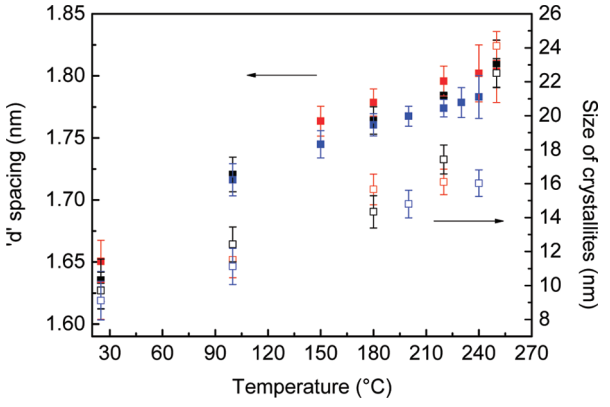

Figure 6. Temperature dependence of interplanar distances (filled symbols) and crystallite size (open symbols) for thick P3HT films on HMDS-treated (red), OTS-treated (black), and untreated (blue) SiO_2.

10 nm at RT by a factor of 2−3 at HT, again independent of surface treatment. On the other hand, after cooling back to RT, the gain in intensity of the *(100)* peak is higher for bare SiO_2 and lower for OTS-treated sample compared to HMDS ones (Figure 4).

Thick Films. In-Plane Measurements. The effect of annealing and slow-cooling on the in-plane structural properties, i.e. along Q_{x-y} is shown in Figure 7A for thick P3HT layers on HMDS-treated substrates. Due to the random orientation of nanocrystallites both the (100) and (020) peaks are visible. After a heating cycle, both peaks show increased intensities. Selected from Figure 7A, the (020) reflection, which is a measure of the $\pi-\pi$ distance between neighbored thiophene

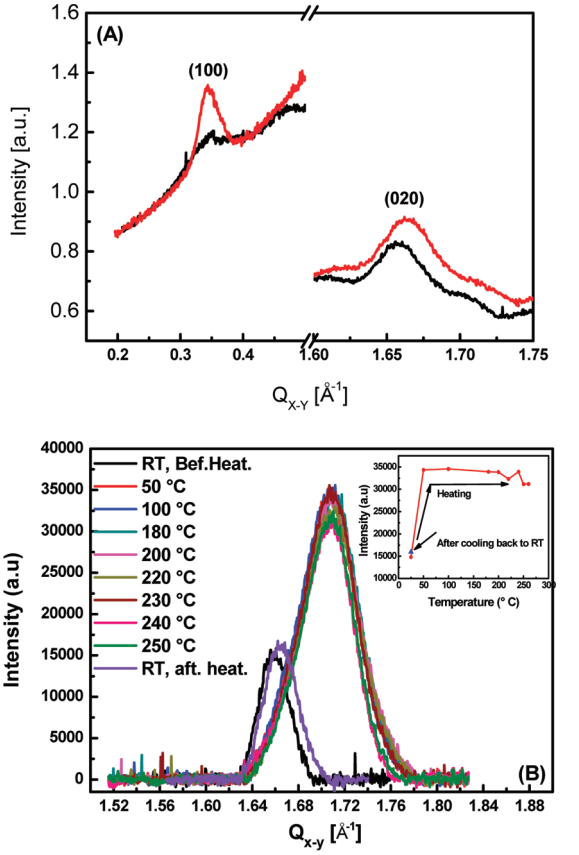

Figure 7. (A) In-plane measurement for a thick P3HT film on a HMDS-treated substrate, before (black line) and after (red line) first annealing, $\alpha_i = 0.15°$, and (B) temperature dependence of the in-plane (020) peak intensity for a thick sample on a HMDS-treated substrate. The inset inside part B shows the change of peak intensity as a function of temperature during heating.

rings, shows again a bimodal behavior as a function of temperature. In contrast to (100) the peak is shifted to higher Q values at higher temperature, i.e., to smaller lattice spacing (Figure 7B). In addition, the (020) peak intensity is increasing with rising temperature, at HT is twice as big compared to RT. In contrast to *a* parameter the change of *b* lattice parameter of a given unit cell is abrupt and takes place at about 50 °C and almost stays constant with increase of temperature (see inset in Figure 7B) indicating a pinning of crystallites at the film−substrate interface. The peak shift from low intense RT position at 1.66 Å^{-1} to a higher intensity HT position with a peak centered at 1.71 Å^{-1} corresponds to a 3% shrinkage of the $\pi-\pi$ distance. In contrast to (100), the peak width of the (020) peak is broader at HT compared to RT indicating a rather reduced in-plane crystallite size. The larger intensity is due to an increased number of crystallites at HT.

Structural Changes in Thin Films. Temperature scans similar to those presented above have been repeated for thin samples with a thickness of about 10 nm. As shown in Figure 8, the (100) out-of plane peak is strongly increased in intensity after the first annealing. The temperature dependence of the *d*-spacing and the crystallite size is shown in Figure 9. The *d*-spacing expands with temperature but the increase is not as strong as was found for the thick layer samples. Independent from the kind of surface treatment, the temperature dependence of the *d*-values at RT is nearly the same and can be described by a thermal expansion coefficient $\alpha_T = 3.5 \times 10^{-4}$ K^{-1}. In contrast to this, the RT value after

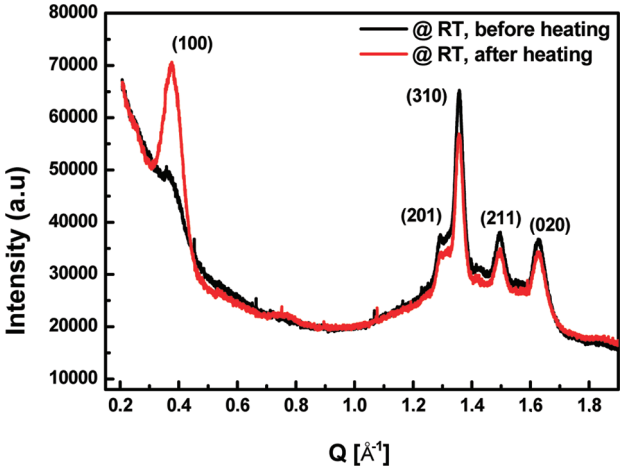

Figure 8. Out-of plane scan of a thin film of HMW P3HT film on a HMDS-treated substrate before (black line) and after (red line) for first annealing.

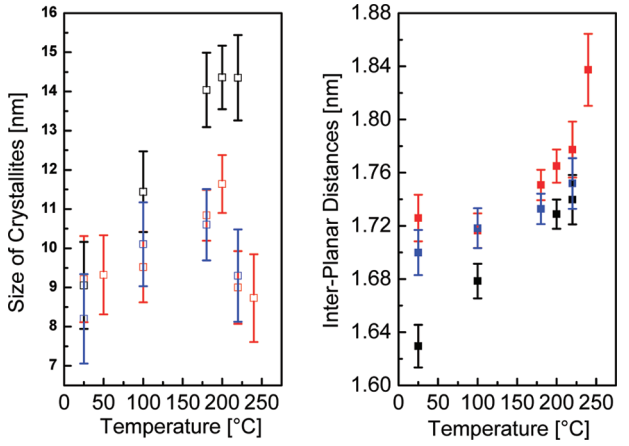

Figure 9. Temperature dependence of interplanar distances (filled symbols) and crystallite size (open symbols) for thin P3HT layers on HMDS-treated (red), OTS-treated (black), and untreated (blue) SiO_2.

slow-cooling differs for the different surface treatments. Whereas OTS-treated films display increasing crystallite size with increase of temperature, HMDS and SiO_2 surfaces seem to be temperature independent.

The in situ temperature dependence of (020) reflection in thin films shows the same bimodal behavior as found for thick layer films (Figure 10). The (020) peak is shifted to the exactly same value at HT as found for thick layer samples and the peak width is enlarged. Again the jump in peak position appears at about 50 °C and stays same for further heating. The decay found at high temperatures may be caused by the influence of the air−film interface.

Thick Films versus Thin Films. A Depth-Resolved Analysis. The influence of the air−film interface on thick films was probed by the depth dependent out-of plane scattering by tuning the angle of incidence. To do this, the intensity of the out-of-plane (100) diffraction peak taken at $\alpha_i < \alpha_{cf}$ was compared to those measured at $\alpha_i \geq \alpha_{cs}$. In the first case the information stems from the first 10 nm straight below the surface of the thick film, while in the latter case the whole film is probed including the buried film- substrate interface (for more details see the Experimental Section). Figure 11 shows the (100) peak intensity as a function of the X-ray incidence angle at various temperatures for an OTS-treated thick film. Probing the bulk ($\alpha_i = 0.30°$) the peak intensity increases

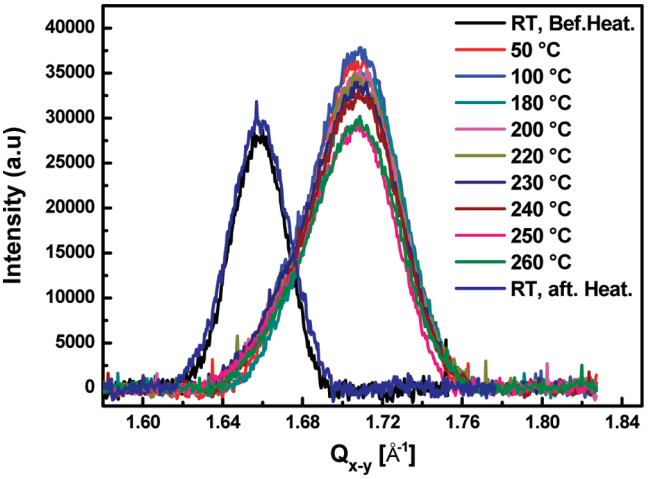

Figure 10. Temperature dependent variation of the in-plane (020) peak for a thin sample on a HMDS-treated substrate, $\alpha_i = 0.15°$.

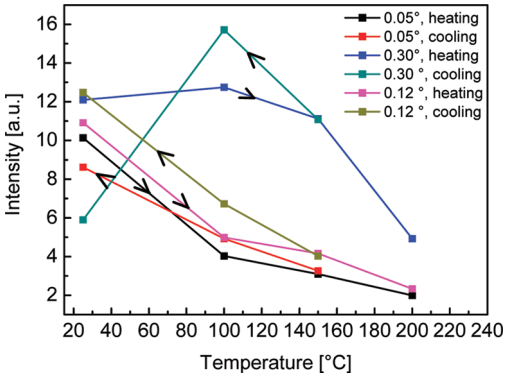

Figure 11. Temperature dependence of the out-of-plane (100) peak intensity for a thick P3HT layer on an OTS-treated substrate at different angles of incidence.

between RT and 100 °C followed by a decrease at higher temperatures. This behavior is principally reversible upon cooling except that the final intensity at RT is at half the value of the original sample. For all other incident angles ($\alpha_i < 0.30°$) the curves show a continuous decrease in intensity for increasing temperature as found for thin films. The same behavior was found for thin films and reveals that the continuous decrease of intensity with increasing temperature for $\alpha_i < \alpha_i^s$ causes temperature-induced morphological changes at the air−film interface. Therefore, the differences in RT values before and after annealing could be due to the change in a particular surface morphology.

Electrical Characterizations

The mobility of thick and thin films based OFETs was measured in situ as a function of the temperature (Figures 12 and 13). As an example, we present the development of the OFET characteristics during a full temperature scan for thin samples on a HMDS-silanized substrate (in the Supporting Information). Generally, the characteristics get blurred toward the maximum temperature of all samples. The source-drain current becomes lower, accompanied by increasing hysteresis effects in both the output and the transfer characteristics. Upon cooling back to room temperature, the characteristics recover almost completely. However, a negative shift of the threshold voltage is irreversible (see below for a discussion).

In thick films, the mobility remains rather constant within a temperature range from room temperature to about 100 °C

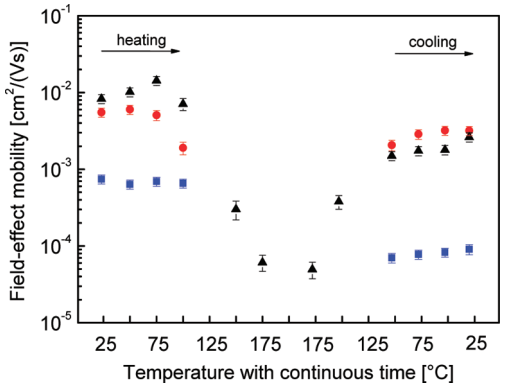

Figure 12. Temperature-dependent hole mobility in thick P3HT field-effect devices, measured in situ in a cyclic procedure of heating from room temperature to 150 °C (186 °C for OTS treatment), followed by cooling back. Different treatment of the insulator-semiconductor interface using untreated SiO_2 (blue symbols), silanized SiO_2 by 26 h immersion in a HMDS atmosphere (red symbols), and silanized SiO_2 by 10 min immersion into OTS (black symbols).

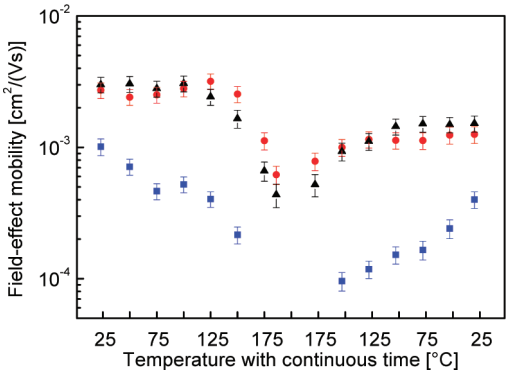

Figure 13. Temperature-dependent hole mobility in thin P3HT field-effect devices (1 mg/mL), measured in situ in a cyclic procedure of heating from room temperature to 186 °C (175 °C for untreated SiO_2), followed by cooling back. Different treatment of the insulator-semiconductor interface using untreated SiO_2 (blue symbols), silanized SiO_2 by 26 h immersion in a HMDS atmosphere (red symbols), and silanized SiO_2 by 10 min immersion into OTS (black symbols).

(Figure 12) followed by a sharp drop above 100 °C, independent of the surface treatment. In the case of nontreated and HMDS-silanized samples, the OFET devices even lose their transistor behavior at around 100 °C. For the OTS-treated interface, the device remains operable until 186 °C. Apart from this particular result, HMDS and OTS treatments yield the same results in terms of the absolute value and the temperature dependence of the field-effect mobility for thick and for thin films. Note that, in thick films, the final mobilities of the silanized samples almost recover the value of the initial mobility, while the mobility in nonsilanized OFETs develops into a significantly lower value after the measurement procedure.

Surprisingly, the thin OFET devices appear to be significantly more temperature stable compared to their thick counterparts (Figure 13). The field-effect mobility remains roughly constant until 150 °C in the case of the silanized samples. At higher temperatures the mobility drops by approximately 1 order of magnitude, but the silanized devices are still operable even at the maximum temperature of 186 °C. For the devices with a nontreated SiO_2 interface, the mobility decreases continuously starting from room temperature. Above 150 °C no reasonable transistor behavior can be observed. After the films cool back to RT, the mobilities are almost half of the initial mobility for both silanized and nonsilanized devices. Therefore, electrical measurements reveal that despite the fact that annealing improves crystallization, the mobility of the film is decreasing. Therefore, charge carrier mobility is mostly caused by interconnecting of these crystallites amorphous regions.

Note that in the literature, the temperature dependence of field-effect mobility in polymer layers is usually studied below room temperature, i.e., in a regime where morphological changes are absent in most cases.[35−39] Therefore, a temperature-activated mobility is found due to the hopping transport in these systems. We have studied the temperature dependence of mobility in a regime starting from room temperature up to the melting point. Within this regime most polyalkylthiophene layers exhibit a temperature-induced change in the molecular conformations, leading to a more twisted backbone and, concurrently, a decrease of the conjugation lengths. This is evident by observing a blue-shift in optical absorption, called "thermochroism".[40−42] From this perspective, these temperature-induced conformational changes should impair charge transport, with the consequence that the thermal activation is overcompensated and the mobility even decreases. The results from X-ray measurements shown in this paper clearly reveal structural changes well below the melting transition of the studied P3HT, and it is plausible to assume that these also affect the motion of charges along and between the crystallites.

A discussion of possible contact effects, as well as typical OFET characteristics, is given in the Supporting Information. Most importantly, the OFET output and transfer characteristics follow the Shockley transistor model at all temperatures. A change in the qualitative behavior during or after temperature treatment is not observed for our samples apart from a permanent increase of gate voltage threshold to −30 V. This shift is irreversible (and remains after cooling back to RT), while the mobility recovers almost completely in most cases.

An occasional slight reduction of the field-effect mobility after passing the temperature protocol compared to its initial value might be due to the diffusion of gold atoms, of which the source and the drain consist, into the polymer layer at high temperatures. Because of the top-contact geometry of the OFET devices, it is possible that the gold atoms diffuse into the polymer layer at elevated temperatures due to the diffusive motion of the gold atoms and the polymer molecules, possibly assisted by the electric field during the measurements. This could result in poorer electrical contact of the source and drain electrodes with the organic layer as well as morphological changes in the polymer layer in the proximity of the contact. The contact resistance in polymer FETs was found to decrease with increasing temperature[43,44] and thus cannot be responsible for the decrease of mobility at high temperatures. We conclude that the dependence of the mobility on temperature is mostly related to the layer morphology and only weakly affected by contact effects.

Finally, we note that the initial room temperature mobility of the silanized devices is considerably higher for a thicker polymer layer. This contrasts with our recent experiments on a P3HT fraction with rather low molecular weight.[7] Here, the field effect mobility was found to be independent of layer thickness. The result was attributed to the existence of an ultrathin well-ordered polymer layer at the polymer-insulator-interface, whose structural parameters determine the charge transport independent of the total thickness of the organic semiconductor. In contrast, Wagner et al. recently observed that the OFET mobility decreases rapidly with decreasing layer thickness for high molecular weight P3HT.[31] On the basis of a detailed analysis of the transistor characteristics, this effect was attributed to a larger energetic disorder at the relevant interface in the case of thin layers.

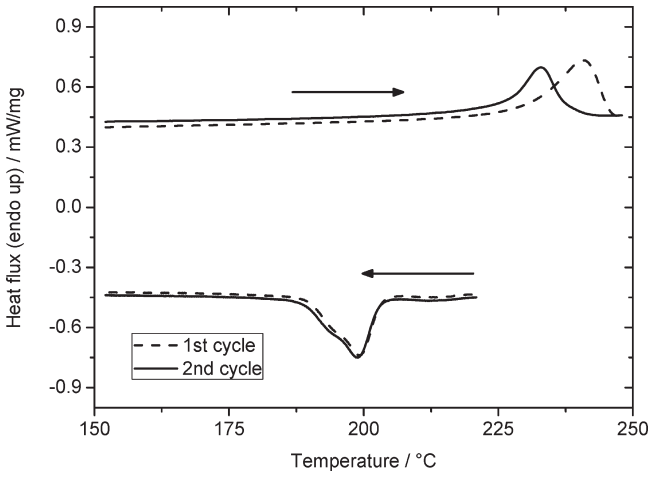

Figure 14. DSC thermograms of high molecular weight P3HT powder, during first (dashed lines) and second (solid lines) temperature cycle.

Discussions

Systematic structure and mobility investigations as a function of temperature have been performed. We have shown that spin-coated samples of P3HT HMW fraction at room temperature undergo significant changes in morphology and structure of nanocrystallites during annealing. In addition, these thermally induced changes differ for thin films (about 10 nm) and thick films (about 200 nm). Finally, the influence of the film−substrate interface becomes evident comparing OTS- and HMDS-treated and untreated SiO_2 substrates.

All these changes can be classified into three points: First, our temperature-dependent experiments give evidence that at elevated temperatures structural ordering is better than at RT. We found a bimodal behavior of the in-plane lattice parameter of unit cell, one at RT and the other at HT which becomes entirely reversible after several heating cycles. In contrast to this, the out-of plane lattice parameter shows continuous variation with temperature and is also reversible. For technologically relevant films of HMW P3HT with a thickness larger than 100 nm the number of nanocrystallites and its degree of preferential orientation is more pronounced at the HT phase, i.e., at a temperature close to 200 °C. As shown by a DSC measurement (Figure 14), melting and crystallization properties of our batch are typical for regioregular P3HT with an endothermic melting peak nearly at 235 °C upon heating and exothermic crystallization at about 190 °C.[32] Following the arguments in Malik et al.,[33] the bulk melting point should be ca. 225 °C. Thus, the structural changes disclosed by our X-ray studies occur at significantly lower temperatures than the melting of the polymer crystals.

The second interesting observation is that the (020) reflection stays visible even at 260 °C, which is above the melting temperature of bulk material.

Moreover, we can characterize this high temperature structure as a thermotropic phase appearing in addition to the phase found at RT. It is possible to transform the system into equilibrium by a first heating cycle and then switch between both phases repeatedly. However, in the high temperature phase the fwhm is smaller but the peak intensity is higher compared to the RT phase. Additionally, considering the change of the in-plane (020) Bragg peak, we find that the in-plane crystallite size becomes smaller at HT compared to RT but the number of crystallites is increased (Figure 7B). Both these phenomena can be explained by a model where crystals existing at RT grow in height at the cost of their lateral width and by collecting chains in their close vicinity, the crystals are accompanied by nucleation of new small crystallites at the film−substrate interface. This scenario is supported by our results obtained for thin films. Here the vertical size of crystallites can grow to reach total film thickness. However, the in-plane behavior is the same as for thick films: the number of in-plane crystals at HT is larger than at RT. This is a hint of the strong influence of the interface on the structural order as suggested by our measurements at low molecular weight P3HT material.[7]

A third finding concerns the unit cell and the thermal changes of lattice parameters. The unit cell of the HMW fraction is similar to the LMW with slightly larger a (alkyl side chains) and b ($\pi-\pi$ stacking) lattice parameters. For thick films we find an expansion of the out-of plane spacing at HT accompanied by compression of in-plane lattice parameter. These changes can be associated with a stretching of alkyl chains but a smaller $\pi-\pi$ distance of the thiophene rings. The same changes in $\pi-\pi$ distance are observed for thin films while the out-of plane d-spacing and size of crystallites do not expand much compared to thick films. Temperature treatment strongly influences the crystalline ordering along the alkyl side chains and has only a moderate influence on the tilted polymer chains and the $\pi-\pi$ stacking.

These structural changes may have consequences for electrical properties. Thus, we like to discuss the temperature dependence of the mobility in relation to the changes in the relevant structural parameters. This correlation might also help to understand the process ultimately limiting the charge transport in P3HT-based transistors. In general, we find a drop in charge carrier mobility for temperatures above 120 °C. Depending on the kind of silanization, the OFET behavior can even disappear completely at elevated temperatures. At first glance, this seems to be contradictory to the expectations from the structural studies. Here, the in-plane measurements clearly show a decrease in the $\pi-\pi$ stacking distance upon heating, which shall assist the charge transport within the crystalline regions. Also, the growing number of crystallites in the in-plane direction, i.e. in the direction of charge transport in an OFET, should be beneficial for charge transport along the substrate plane. For clarification of this apparent conflict, we would like to point out that solid layers formed from long crystallizable polymer chains as P3HT generally exhibit a multiphase morphology, with crystalline domains separated by amorphous regions.[12,17,32] Though the domain boundaries are often hard to distinguish in layers of high MW P3HT, there is evidence that the crystalline regions constitute only a fraction of the whole samples volume. The DSC analysis of a P3HT fraction with a molecular weight M_n of 27000 g/mol revealed that the material had a crystallinity of only 18 vol %.[8] Despite this, the room temperature mobility in layers of P3HT with high molecular weight and regioregularity is quite considerable. It has, therefore, been proposed that long polymer chains bridge the regions between crystalline domains, allowing the charges to move efficiently between them.[11] Another explanation is based on HR-TEM observations of strong interconnection by bridging tie-crystallites.[17]

Our structural and electrical measurements indicate that the strong reduction of the macroscopic mobility—comprising the charge transport over numerous of domains—above a certain temperature cannot be explained by thermally induced morphological changes within the well-ordered crystalline domains but that this effect must be caused by a pronounced decrease of the intergrain transport. Our studies provide strong evidence that the crystallite size along the (020) direction becomes smaller, due to shrinkage of the $\pi-\pi$ stacking. Since the whole channel area between source and drain contact is constant, this process will diminish the amount of crystalline material accessible for the carriers during in-plane transport in the OFET. In accordance with this interpretation the effect of temperature on the OFET mobility is far more pronounced in thick layers. Here, the size of the crystallites was shown to increase substantially in the vertical (100)-direction, probably on expense of their lateral width.

Therefore, transport properties of HMW P3HT films might be influenced by temperature induced changes of intercrystalline regions.

Finally, the macroscopic charge transport, as it is present in OFETs, is crucially determined by the presence and especially by the extent of amorphous domains within the path of the carriers. It is, therefore, not surprising that the temperature dependence of the charge carrier mobility is only indiscernible related to thermally induced changes in the structure of the crystallites.

Acknowledgment. This work was supported by DFG (Priority Program 1121), S.J. thanks BASF for financial support. We thank beamline scientists at BL9, DELTA, and ID 10B, ESRF, for experimental support.

Supporting Information Available: Text discussing the AFM investigation and preparation of OFET samples, extraction and temperature-depedence of field effect mobility and figures showing the AFM topography of the thick P3HT layers, in situ OFET characteristics during one cycle of thermal treatment, scheme of the electrical bonding for measuring the OFET characteristics, and theoretical output and transfer characteristics. This material is available free of charge via the Internet at http://pubs.acs.org.

Note Added after ASAP Publication. This article was published ASAP on June 11, 2009. A value has been changed in the first paragraph of the Introduction section. The correct version was published on June 17, 2009.

References and Notes

(1) Katz, H. E. *Chem. Mater*. **2004**, *16*, 4748–4756.
(2) Chabinyc, M. L.; Salleo, A. *Chem. Mater*. **2004**, *16*, 4509–4521.
(3) Sirringhaus, H; Brown, P J; Friend, R H; NielsenM, M; Bechgaard, K; Langeveld-Voss, B M W; Spiering, A J H; Janssen, R A J; Meijer, E W; Herwig, P; de Leeuw, D M *Nature* **1999**, *401*, 685–688.
(4) Ong, B. S.; Wu, Y.; Liu, P.; Gardner, S. *J. Am. Chem. Soc*. **2004**, *126*, 3378–3379.
(5) McCulloch, I.; Heeney, M.; Bailey, C.; Genevicius, K.; Macdonald, I.; Shkunov, M.; Sparrowe, D.; Tierney, S.; Wagner, R.; Zhang, W.; Chabinyc, M. L.; Kline, R. J.; McGehee, M. D.; Toney, M. F. *Nat. Mater*. **2006**, *5*, 328–333.
(6) Joshi, S.; Grigorian, S.; Pietsch, U. *Phys. Stat. Solidi A* **2008**, *205*, 488–496.
(7) Joshi, S.; Grigorian, S.; Pietsch, U.; Pingel, P.; Zen, A.; Neher, D.; Scherf, U. *Macromolecules* **2008**, *41*, 6800–6808.
(8) Zen, A.; Saphiannikova, M.; Neher, D.; Grenzer, J.; Grigorian, S.; Pietsch, U.; Asawapirom, U.; Janietz, S.; Scherf, U.; Lieberwirth, I.; Wegner, G. *Macromolecules* **2006**, *39*, 2162–2171.
(9) Zen, A.; Pflaum, J.; Hirschmann, S.; Zhuang, W.; Jaiser, F.; Asawapirom, U.; Rabe, J. P.; Scherf, U.; Neher, D. *Adv. Funct. Mater*. **2004**, *14*, 757–764.
(10) Kline, R. J.; McGehee, M. D.; Kdnikova, E. N.; Liu, J.; Frechet, J. M. *J. Adv. Mater*. **2003**, *15*, 1519–1522.
(11) Kline, R. J.; McGehee, M. D.; Kadnikova, E. N.; Liu, J.; Frechet, J. M. J.; Toney, M. F. *Macromolecules* **2005**, *38*, 3312–3319.
(12) Kline, R. J.; McGehee, M. D.; Toney, M. F. *Nature Mat*. **2006**, *5*, 222–228.
(13) Abbel, R.; Schenning, A. P. H. J; Meijer, E. W. *Macromolecules* **2008**, *41*, 7497–7504.
(14) Majewski, L. A.; Kingsley, J. W.; Balocco, C.; Song, A. M. *Appl. Phys. Lett*. **2006**, *88*, 222108–222110.
(15) Kim, D. H.; Park, Y. D.; Jang, Y.; Yang, H.; Kim, Y. H.; Han, J. I.; Moon, D. G.; Park, S.; Chang, T.; Chang, C.; Joo, M.; Ryu, C. Y.; Cho, K. *Adv. Funct. Mater*. **2005**, *15*, 77–82.
(16) Brinkmann, M.; Rannou, P. *Adv. Funct. Mater*. **2007**, *17*, 101–108.
(17) Brinkmann, M.; Rannou, P. *Macromolecules* **2009**, *42*, 1125–1130.
(18) Kline, R. J.; DeLongchamp, D. M.; Daniel, R.; Fischer, A.; Jung, Y.; Lin, E. K.; Richter, L. J.; McCulloch, I. *Macromolecules* **2007**, *40*, 7960–7965.
(19) Pingel, P.; Zen, A.; Neher, D.; Lieberwirth, I.; Wegner, G.; Allard, S.; Scherf, U.; *Appl. Phys. A: Mater. Sci. Process*. **2009**, 67−72.
(20) Abdou, M. S. A.; Lu, X.; Xie, Z. W.; Orfino, F.; Deen, M. J.; Holdcroft, S. *Chem. Mater*. **1995**, *7*, 631.
(21) Grecu, S.; Roggenbuck, M.; Opitz, A.; Brutting, W. *Org. Electron*. **2006**, *7*, 276–286.
(22) Bao, Z.; Dodabalapur, A.; Lovinger, A. J. *Appl. Phys. Lett*. **1996**, *69*, 4108–4110.
(23) Werzer, O.; Matoy, K.; Strohriegl, P.; Resel, R. *Thin Solid Films* **2007**, *515*, 5601–5605.
(24) Kim, D. H.; Jang, Y.; Park, Y. D.; Cho, K. *Macromolecules* **2006**, *39*, 5843.
(25) DeLongchamp, D. M.; Kline, R. J.; Jung, Y.; Lin, E. K.; Fischer, D. A.; Gundlach, D. J.; Cotts, S. K.; Moad, A. J.; Richter, L. J.; Toney, M. F.; Heeney, M.; McCulloch, I. *Macromolecules* **2008**, *41*, 5709–5715.
(26) Loewe, R. S.; Khersonsky, S. M.; Mc Cullough, R. D. *Adv. Mater*. **1999**, *11*, 250–253.
(27) Trznadel, M.; Pron, A.; Zagorska, M.; Chrzaszcz, R.; Pielichowski, J. *Macromolecules* **1998**, *31*, 5051–5058.
(28) Chabinyc, M. L.; Toney, M. F.; Kline, J. K.; McCulloch, I.; Heeney, M. *J. Am. Chem. Soc*. **2007**, *129*, 3226–3237.
(29) Tashiro, K.; Keiko, O.; Yasuhisa, M.; Masamichi, K.; Tsuyoshi, K.; Katsumi, Y. *J. Polym. Sci., Part B: Polym. Phys*. **1991**, *29*, 1223–1233.
(30) Prosa, T. J.; Moulton, J.; Heeger, A. J.; Winokur, M. J. *Macromolecules* **1999**, *32*, 4000–4009.
(31) Wagner, V. et al. Poster presented at the MRS Spring Meeting, 2008, San Francisco, CA, **2008**.
(32) Hugger, S.; Thomann, R.; Heinzel, T.; Thrun-Albrecht, T. *Colloid Polym. Sci*. **2004**, *282*, 932.
(33) Malik, S.; Nandi, A. K. *J. Polym. Sci., Part B: Polym. Phys*. **2002**, *40*, 2073.
(34) Prosa, T. J.; Winokur, M. J.; Moulton, J.; Smith, P.; Heeger, A. J. *Macromolecules* **1992**, *25*, 4364–4372.
(35) Blom, P. W. M.; , deJong, M. J. M.; vanMunster, M. G. *Phys. Rev. B* **1997**, *55*, R656−R659.
(36) Burgi, L.; Sirringhaus, H.; Friend, R. H. *Appl. Phys. Lett*. **2002**, *80*, 2913−2915.
(37) Mozer, A.J.; Sariciftci, N. S. *Chem. Phys. Lett*. **2004**, *389*, 438−442.
(38) Sirringhaus, H.; Wilson, R. J.; Friend, R. H.; Inbasekaran, M.; Wu, W.; Woo, E. P.; Grell, M.; Bradley, D. D. C. *Appl. Phys. Lett*. **2000**, *77*, 406−408.
(39) Vissenberg, M.; Matters, M. *Phys. Rev. B* **1998**, *57*, 12964−12967.
(40) Garreau, S.; Leclerc, M.; Errien, N.; Louarn, G. *Macromolecules* **2003**, *36*, 692−697.
(41) Inganas, O.; Salaneck, W. R.; Osterholm, J. E.; Laakso, J. *Synth. Met*. **1988**, *22*, 395−406.
(42) Yang, C.; Orfino, F. P.; Holdcroft, S. *Macromolecules*. **1996**, *29*, 6510−6517.
(43) Burgi, L.; Richards, T. J.; Friend, R. H.; Sirringhaus, H. *J. Appl. Phys*. **2003**, *94*, 6129−6137.
(44) Hamadani, B. H.; Natelson, D. *Appl. Phys. Lett*. **2004**, *84*, 443−445.